Received 28 March 2024; revised 4 May 2024; accepted 22 May 2024. Date of publication 29 May 2024; date of current version 28 June 2024.

Digital Object Identifier 10.1109/OJCOMS.2024.3406819

Efficient Parallel PAPR Reduction Method Using Null-Constrained Peak Cancellation Signal for Massive MIMO-OFDM Systems

JUN SAITO, (Graduate Student Member, IEEE), TAKANORI HARA, (Member, IEEE), AND KENICHI HIGUCHI, (Senior Member, IEEE)

Graduate School of Science and Technology, Tokyo University of Science, Noda 278-8510, Chiba, Japan

CORRESPONDING AUTHOR: J. SAITO (e-mail: 7322547@ed.tus.ac.jp)

ABSTRACT In this paper, we propose new methods for reducing the peak-to-average power ratio (PAPR) for downlink massive multiple-input multiple-output (MIMO) along with orthogonal frequency division multiplexing. We develop the PAPR reduction method based on peak cancellation (PC) signals using the null space in a MIMO channel, which can prevent in-band distortion at the receiver while reducing the PAPR of the transmitted signal. The proposed method concurrently performs the PC signal-based PAPR reduction process using the small number of transmitter antennas by dividing them into multiple blocks. Although this method leverages the low-dimensional null space in the MIMO channel, it facilitates PAPR reduction while suppressing the degradation of the bit error rate (BER) and reducing the required computational complexity. Furthermore, we introduce the generation of PC signals that suppress the multiple peaks of the original transmitted signal in the time domain, further reducing the computational complexity in the PAPR reduction process. Computer simulation results show that the proposed method significantly reduces the computational complexity and improves the BER and convergence rate of the PAPR.

INDEX TERMS Massive multiple-input multiple-output (MIMO), null space, orthogonal frequency division multiplexing (OFDM), peak-to-average power ratio (PAPR) reduction.

I. INTRODUCTION

IN FUTURE wireless communications systems such as 6G, the demand for data will be extremely high. Terahertz (THz) communication have been a promising technology for utilizing wide bandwidths. However, the signal in THz communications suffers from very high path loss [1]. As a solution to this problem, multiple-input multiple-output (MIMO) with orthogonal frequency-division multiplexing (OFDM) transmission has attracted considerable attention.

Massive MIMO transmission is a promising technology [2], [3]. Massive MIMO—wherein the base station (BS), which has a large number of antennas—serves a small number of users with beamforming (BF) in the downlink, which is important for extending the range of mobile broadband without a multi-user interference (MUI). In addition, a channel with a wide bandwidth becomes a frequency-selective channel owing to the delay spread. OFDM transmission is an effective method for handling frequency-selective channels owing to the reduction in the symbol rate and the application of cyclic prefixes. Therefore, a combination of massive MIMO transmissions and OFDM signals is essential for realizing a mobile broadband with a wide coverage.

However, a high peak-to-average power ratio (PAPR) is important for massive MIMO-OFDM transmissions. When the PAPR of the transmitted signal is high, in-band distortion and out-of-band radiation (OBR) occur owing to the nonlinearity in the power amplifier. To realize massive MIMO, the size and cost of the power amplifier for each transmission antenna should be low, which results in weak linearity. Therefore, PAPR reduction is a crucial challenge for realizing massive MIMO-OFDM transmissions.

A. RELATED WORK

In a multiuser (MU) massive MIMO downlink scenario, many PAPR reduction schemes that do not require any

processing at each receiver (user terminal) side owing to the spatial distribution have been actively investigated. They comprise the use of various techniques, such as tone reservation [4], antenna reservation [5], optimization-based approaches [6], [7], [8], [9], learning-based approaches [10], [11], [12], superimposed training-based approaches [13], [14], and methods comprising the use of the null space in a MIMO channel [15], [16], [17], [18], [19], [20], [21], [22], [23]. We note that the optimization-based methods in [7] and [8] also use the null space in a MIMO channel, and learning-based and superimposed training-based approaches can be further explored in future works.

In [4] and [5], PAPR reduction methods were proposed in which certain tones and transmitter antennas were exclusively dedicated to PAPR reduction, respectively. These methods can be applied with low computational complexity and can eliminate the in-band interference caused by the PAPR reduction signal on the receiver side. However, they reduce the PAPR of the transmitted signal at the cost of the frequency and spatial efficiency of massive MIMO-OFDM transmission.

A number of optimization-based approaches have been investigated as PAPR reduction methods that can circumvent the loss of frequency and spatial efficiency. They are based on various methods such as the fast iterative truncation [6], alternative direction method of multipliers [7], gradient descent method [8], and alternating projection method [9]. Owing to the tailored formulation of the PAPR reduction problem, these approaches can realize a low PAPR while suppressing or circumventing MUI and OBR. In particular, the method in [8], namely the MU precoding based PAPR reduction via gradient descent approach (MU-PP-GDm) algorithm, improves the PAPR reduction capability and realizes a lower computational complexity compared to the schemes in [6] and [7]. However, the MU-PP-GDm algorithm still has high computational complexity owing to the use of singular value decomposition (SVD).

As with optimization-based approaches, PAPR reduction methods with the null space in a MIMO channel can use all transmission bandwidths and transmitter antennas for data transmission. Furthermore, they can avoid the degradation of the bit error rate (BER) due to in-band interference and MUI by restricting the PAPR reduction signals to the null space in a MIMO channel. In [15], [16], [17], our research group proposed PAPR reduction methods using the null space in a MIMO channel. The unused beam reservation-based PAPR reduction method was investigated in [18], which is similar to the use of the null space in the MIMO channel, as originally reported in [15], [16], [17].

We have also reported the complexity-reduced PAPR reduction methods based on peak cancellation (PC) signals using the null space in the MIMO channel [19], [20], [21], [22], [23], which is referred to as PC with a channel-null constraint (PCCNC). The original concept of the PC signal-based method was investigated in [24], [25]. In this concept, the transmitter generates a PC signal with a single dominant peak in the time domain, and its transmission bandwidth is equal to that of the OFDM signal. By directly adding the PC signal to the time-domain transmission signal at each transmitter antenna, PAPR reduction is achieved without OBR. In PCCNC, the transmission signals for all the transmitter antennas are jointly considered in the vector form. The PC signal is restricted to the null space in the MIMO channel by the BF vector, thus eliminating the in-band interference on the receiver side. Moreover, the MUI is eliminated with the application of a zero-forcing-based (ZF-based) BF to the data signal, which was also used in [9]. However, PCCNC suffer from high computational complexity and requires a large number of iterations for the convergence of the PAPR reduction. This is because the dimensions of the null space in a massive MIMO channel are very large, which significantly increases the computational complexity in calculating the null space and restricts the PC signals to the null space. Moreover, each iteration of the PCCNC can suppress the peak power only at a single time owing to the PC signal being designed such that it has a single dominant peak in the time domain. As a result, the PCCNC requires a large number of iterations to suppress the PAPR sufficiently. Therefore, the development of a promising PAPR reduction method with even less computational complexity is required.

B. CONTRIBUTIONS

In this paper, we proposed two complexity-reduced PCCNC schemes for MU massive MIMO-OFDM. The contributions of this study are summarized as follows:

- We first developed a PCCNC in which the transmitter antennas are divided into antenna blocks, thus allowing for parallel PAPR reduction for each antenna block. This development enhances the convergence speed of the PAPR reduction and lowers the computational complexity for restriction to the null space owing to a decrease in its dimensions. This advantage is enhanced when the system scales up. It should be noted that the contents of this contribution are partially based on [23] but are extended to accommodate frequency-selective fading channels. In particular, as the addition of the PC signal projected onto the null space in the time-domain MIMO channel may interfere with the data signals owing to multipath delay, the proposed parallel PCCNC operates depending on each subcarrier, differing from the approach in [23].
- In addition, we proposed a PCCNC scheme that can be used to design PC signals with multiple peaks in the time domain per iteration, like the approach in [21]. Each peak of the PC signal plays a role in simultaneously suppressing the peak power of the transmission signal at different times. This scheme suppresses multiple peak powers per iteration, thus enhancing the convergence speed of the PAPR reduction. In this scheme, the PC signals are based on the basic time-domain pulse signal, with a bandwidth

TABLE 1. Key quantities, parameters, and symbols.

N, M	The number of transmitter antennas and receiver antennas
K	The number of subcarriers
F	The number of FFT/IFFT points
Q	The number of iterations
A	The number of antenna blocks
L	The number of peaks to be suppressed per iteration
$\mathbf{x}^{(q)}[t]$	The time-domain data signal vector at time t at q-th iteration
$\mathbf{H}_k$, $\mathbf{V}_k$	The MIMO channel and the null space associated with k-th subcarrier
$\mathbf{H}_{k,a}$, $\mathbf{V}_{k,a}$	The MIMO channel and the null space of antenna block a associated with k-th subcarrier
$g_k[t]$	The basic pulse signal associated with k-th subcarrier
$\tau^{(q)}$	The target time index at q-th iteration
P_{th}	The power threshold
$\tilde{\mathbf{w}}_k^{(q)}$	The ideal BF vector in terms of the PAPR reduction associated with k-th subcarrier
$\mathbf{w}_k^{(q)}$	The BF vector of the PC signal associated with k-th subcarrier
$\mathbf{p}_k^{(q)}[t]$	The PC signal vector based on $g_k[t]$ at q-th iteration
$\bar{\mathbf{p}}^{(q)}[t]$	The average PC signal vector at q-th iteration
$\tilde{\mathbf{w}}_{k,a}^{(q)}$	The ideal BF vector in terms of the PAPR reduction of antenna block a associated with k-th subcarrier
$\mathbf{w}_{k,a}^{(q)}$	The BF vector of the PC signal of antenna block a associated with k-th subcarrier
$\mathbf{p}_{k,a}^{(q)}[t]$	The PC signal vector based on $g_k[t]$ of antenna block a at q-th iteration
$\bar{\mathbf{p}}_a^{(q)}[t]$	The average PC signal vector of antenna block a at q-th iteration
$\tau_l^{(q)}$	The target time index for l-th peak at q-th iteration
$\bar{\mathbf{p}}_l^{(q)}[t]$	The average PC signal vector for l-th peak at q-th iteration

equal to the subcarrier spacing. This differs from the approach in [21], which comprises the use of a roll-off raise-cosine filter.

- We demonstrate that the proposed PCCNC significantly reduces the computational complexity compared with the conventional PCCNC [20] under frequency-selective channels and the MU-PP-GDm algorithm [8]. In particular, as the number of transmitter antennas increases, the proposed PCCNC can realize a lower computational complexity than the MU-PP-GDm, the computational complexity of which is lower than other optimization-based approaches. Furthermore, the proposed method realizes a PAPR performance comparable to that of MU-PP-GDm while suppressing the BER degradation.

C. ORGANIZATIONS AND NOTATION

The remainder of this paper is organized as follows. Section II describes the system model. Sections III and IV describe the conventional PCCNC and the two proposed parallel techniques, respectively. Section V presents the numerical results of the computer simulations, and Section VI presents the conclusions of the paper. For the convenience of the reader, we summarize the most important quantities and parameters used in the paper with corresponding symbols in Table 1.

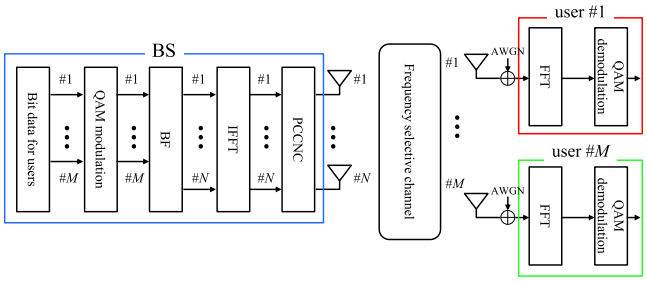

FIGURE 1. System model.

II. SYSTEM MODEL

We assume a downlink MU massive MIMO system with an OFDM signal. Fig. 1 illustrates the system model, wherein a BS transmitter equipped with N antennas serves M single antenna user terminals simultaneously. In this study, it is assumed that N is much larger than M. Let $\mathbf{s}_k$ denote the M-dimensional data stream vector related to the k-th OFDM subcarrier for M users, where $k = 1, \ldots, K$ is an index of the OFDM subcarriers, with K denoting the total number of OFDM subcarriers. Then, $\mathbf{s}_k$ is given as

$$\mathbf{s}_k = \left[s_{k,1} \cdots s_{k,M}\right]^T, \tag{1}$$

where $s_{k,m}$ is the quadrature amplitude modulation (QAM) symbol vector for the m-th user at the k-th subcarrier. To eliminate the MUI, we consider applying the ZF-based BF scheme to the data stream vector $\mathbf{s}_k$. Subsequently, the N-dimensional frequency-domain data signal vector $\mathbf{y}_k$ associated with the k-th subcarrier can be obtained as

$$\mathbf{y}_k = \mathbf{B}_k \mathbf{s}_k = \left[y_{k,1} \cdots y_{k,N}\right]^T, \tag{2}$$

where $y_{k,n}$ and $\mathbf{B}_k$ represent the signal transmitted from the n-th transmitter antenna and $N \times M$-dimensional BF matrix associated with the k-th subcarrier, respectively. The BF process may further enhance the high PAPR of the OFDM signals owing to the difference in the transmission power levels among the transmitter antennas.

After the BF, an inverse fast Fourier transform (IFFT) is applied to the frequency-domain data signal vector. The number of FFT/IFFT points is F. In this study, we consider a four-times oversampling in the time domain, i.e., $F = 4K$. The $F \times K$-dimensional inverse discrete Fourier transform matrix is denoted as $\mathbf{F}^H$. The F-dimensional time-domain signal transmitted from n-th antenna vector $\mathbf{x}_n$ is given by

$$\mathbf{x}_n = \mathbf{F}^H \left[y_{1,n} \cdots y_{K,n}\right]^T. \tag{3}$$

The N-dimensional time-domain data signal vector at time t is given as

$$\mathbf{x}[t] = \left[x_1[t] \cdots x_N[t]\right]^T, \tag{4}$$

where $x_n[t]$ is the transmitted signal from antenna n at time t. Before the transmission over the wireless channel, a cyclic-prefix (CP) is added to the time-domain transmission signals of each antenna to avoid inter-symbol interference (ISI). It

should be noted that for simplicity, Fig. 1 and the descriptions below omit the process associated with the CP.

As the time-domain data signal generated above may have a very high PAPR, a PCCNC-based PAPR reduction is executed. The basic (conventional) PCCNC procedure is described in the following section. As shown in Fig. 1, the PCCNC-based PAPR reduction does not require each user terminal to perform any additional processing.

In this study, we assume a frequency-selective channel. The $M \times N$-dimensional matrix $\mathbf{H}_k$ is the MIMO channel matrix associated with k-th OFDM subcarrier and is expressed as follows:

$$\mathbf{H}_k = \begin{bmatrix} H_{k,11} & \cdots & H_{k,1N} \\ \vdots & \ddots & \vdots \\ H_{k,M1} & \cdots & H_{k,MN} \end{bmatrix}, \tag{5}$$

where $H_{k,mn}$ is the channel between n-th transmitter antenna and the m-th user at the k-th subcarrier.

$$H_{k,mn} = \sum_{d=1}^{D} \alpha_{d,mn} e^{j2\pi \delta_{d,mn} f_k}, \tag{6}$$

where $\alpha_{d,mn}$ and $\delta_{d,mn}$ are the pass loss and delay time of the d-th path between the n-th transmitter antenna and m-th user, respectively. In addition, f_k denotes the frequency of the k-th subcarrier. D is the total number of delay paths. We assume that the channel matrices $\mathbf{H}_k$ are perfectly known at the BS with an ideal channel estimation. Let $\mathbf{V}_k$ denote the $N \times (N-M)$-dimensional matrix corresponding to the null space in a MIMO channel associated with k-th subcarrier $\mathbf{H}_k$. Then, $\mathbf{V}_k$ satisfies $\mathbf{H}_k \mathbf{V}_k = \mathbf{O}$, and all of its N-M column vectors are orthonormalized with each other.

The user terminal receives the transmitted signal added to an additive white Gaussian noise, which follows an independent and identically distributed (i.i.d.) complex Gaussian distribution with zero mean and variance N_0.

III. CONVENTIONAL PEAK CANCELLATION WITH A CHANNEL-NULL CONSTRAINT (PCCNC)

In this section, we describe a conventional PCCNC in a downlink MU massive MIMO-OFDM system in frequency-selective fading channels [20], which is a PAPR reduction method that uses the null space in the MIMO channel. In addition, we summarized the drawbacks of the conventional PCCNC when applied to massive MIMO-OFDM systems.

In this method, the peak power of MIMO-OFDM signals is suppressed by repeatedly adding a PC signal to the time-domain. In addition, as PC signals are restricted to the null space in the MIMO channel, this method prevents PC signals from reducing the PAPR of the transmission signals and degrading the transmission quality.

The process of the conventional method [20] is presented in Fig. 2. This method comprises the use of the PC signal and the null space in a MIMO channel $\mathbf{V}_k$ to suppress the peak power of the MIMO-OFDM signals while avoiding interference with the data stream. The PC signal vector, to which the BF is

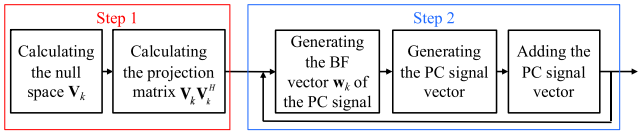

FIGURE 2. Block diagram of the PCCNC.

applied for the suppression of the signal power levels of all the transmitter antennas and the restriction of the signal to the null space in the MIMO channel, is added to the transmission signal repeatedly. At the q-th iteration, the purpose of the PCCNC is that the peak power of the transmission signal observed at the time index $\tau^{(q)}$ is suppressed by the addition of the PC signal. To realize this purpose, the following two steps are performed for the PCCNC.

- Step 1: Calculate the null space $\mathbf{V}_k$ and projection matrix onto the null space $\mathbf{V}_k\mathbf{V}_k^H$ for all $k = 1, \ldots, K$.
- Step 2: Addition of the PC signal vector, which is restricted to the null space in the MIMO channel, to the transmission signal vector.

The purpose of step 1 is to introduce the projection matrix in advance to be used for the null constraint. It is necessary to execute many iterations of step 2 for significant PAPR reduction.

In the following section, we describe the details of the signal processing of the conventional PCCNC at the q-th iteration. In the PC signal vector generation process, the basic time-domain pulse signal $g_k[t]$, having a bandwidth equal to the subcarrier spacing and center frequency, is equal to the frequency of the k-th subcarrier f_k. $g_k[t]$ is given by

$$g_k[t] = h[t] e^{j2\pi f_k t}, \tag{7}$$

where $h[t]$ is the frequency transfer function of $g_k[t]$, which is equivalent to the ideal rectangular function. In particular, $h[t] = 1$ when $t = 0, \ldots,$ F-1. Thus, $g_k[t]$ is a sinc function in the time domain, the peak amplitude of which is 1.0 at $t = 0$ with subcarrier-dependent complex phase rotation. In addition, $g_k[t]$ has an OBR of zero for baseband transmission signals.

The time-domain transmission signal vector at the q-th iteration of the PCCNC ($q = 1, \ldots, Q$) at time t is $\mathbf{x}^{(q)}[t] = \begin{bmatrix} x_1^{(q)}[t] & \cdots & x_N^{(q)}[t] \end{bmatrix}^T$. $\mathbf{x}^{(q)}[t]$ is initialized as the original data signal vector, where $\mathbf{x}^{(1)}[t] = \mathbf{x}[t]$. The target time index $\tau^{(q)}$ for the PCCNC at the q-th iteration is determined based on $\mathbf{x}^{(q)}[t]$. In particular, $\tau^{(q)}$ is the time index wherein $x_n^{(q)}[t]$ for all $n = 1, \ldots, N$ and $t = 0, \ldots, F-1$ has the maximum power over the power threshold P_{th}. The PC signal vector at the q-th iteration based on $g_k[t]$, $\mathbf{p}_k^{(q)}[t]$, is generated as

$$\mathbf{p}_k^{(q)}[t] = \mathbf{w}_k^{(q)} g_k[t - \tau^{(q)}], \tag{8}$$

where $\mathbf{w}_k^{(q)}$ is the BF vector of the PC signal associated with the k-th subcarrier. $\mathbf{p}_k^{(q)}[t]$ suppresses the peak power at $\tau^{(q)}$ while being restricted to the null space in the MIMO

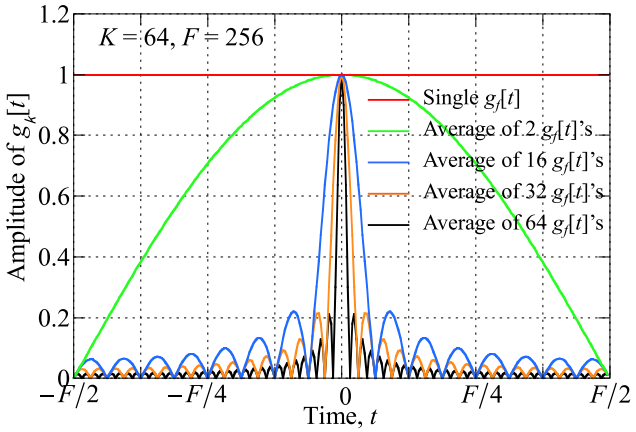

FIGURE 3. Basic time-domain pulse signal.

channel. $\mathbf{p}_k^{(q)}[t]$ is generated by multiplying $\mathbf{w}_k^{(q)}$ to the $\tau^{(q)}$-time-shifted version of $g_k[t]$ and prevents the OBR and interference with the data stream. This is because the PC signal does not appear at the receiver side owing to the transmission of the PC signal only through the null space in the MIMO channel.

First, for generating $\mathbf{w}_k^{(q)}$, an ideal BF vector in terms of the PAPR reduction $\widetilde{\mathbf{w}}_k^{(q)}$ is designed such that the peak power of $\mathbf{x}^{(q)}[t]$ is suppressed to P_{th}. Subsequently, $\widetilde{\mathbf{w}}_k^{(q)}$ is projected onto the null-space $\mathbf{V}_k$ in the MIMO channel. $\widetilde{\mathbf{w}}_k^{(q)}$ and $\mathbf{w}_k^{(q)}$ can be expressed as follows:

$$\widetilde{\mathbf{w}}_k^{(q)} = [\widetilde{w}_{k,1}^{(q)} \quad \cdots \quad \widetilde{w}_{k,N}^{(q)}]^T, \tag{9}$$

where $\widetilde{w}_{k,n}^{(q)}$ is given by

$$\widetilde{w}_{k,n}^{(q)} = \begin{cases} \sqrt{P_{\text{th}}} e^{j\theta_n^{(q)}[\tau^{(q)}]} - x_n^{(q)}[\tau^{(q)}], & \left|x_n^{(q)}[\tau^{(q)}]\right|^2 > P_{\text{th}} \\ 0, & \text{Otherwise}, \end{cases} \tag{10}$$

where $\theta_n^{(q)}[\tau^{(q)}]$ is the phase of $x_n^{(q)}[\tau^{(q)}]$. If $\widetilde{\mathbf{w}}_k^{(q)}$ in (9) is used as $\mathbf{w}_k^{(q)}$ in (8), the power levels of the transmission signals for all N antennas at time $\tau^{(q)}$ can be equal to or less than P_{th}. However, as $\widetilde{\mathbf{w}}_k^{(q)}$ has a component that is orthogonal to the null space in the MIMO channel, the PC signal vectors interfere with the data streams. Therefore, $\widetilde{\mathbf{w}}_k^{(q)}$ is projected onto the null space in the MIMO channel to generate $\mathbf{w}_k^{(q)}$ as follows:

$$\mathbf{w}_k^{(q)} = \mathbf{V}_k \mathbf{V}_k^H \widetilde{\mathbf{w}}_k^{(q)}. \tag{11}$$

However, one problem with the use of use of $\mathbf{p}_k^{(q)}[t]$ is that, as the bandwidth of $g_k[t]$ is narrower compared to that of the transmission signal, the side lobe of $\mathbf{p}_k^{(q)}[t]$ in the time domain is wider. To address this issue, the conventional PCCNC averages $\mathbf{p}_k^{(q)}[t]$ for all $k = 1, \ldots, K$. As the effective bandwidth of the averaged PC signal is increased by the averaging process, the side lobe in the time domain becomes narrower, as shown in Fig. 3. The average PC signal vector $\overline{\mathbf{p}}^{(q)}[t]$ is generated as

$$\overline{\mathbf{p}}^{(q)}[t] = \frac{1}{K} \sum_{k=1}^{K} \mathbf{p}_k^{(q)}[t]. \tag{12}$$

In the q-th iteration of the PCCNC, the average PC signal vector $\overline{\mathbf{p}}^{(q)}[t]$ is added to $\mathbf{x}^{(q)}$ to reduce the PAPR as follows:

$$\mathbf{x}^{(q+1)}[t] = \mathbf{x}^{(q)}[t] + \overline{\mathbf{p}}^{(q)}[t]. \tag{13}$$

Although the conventional PCCNC can effectively reduce the PAPR of the transmission signals in a MIMO-OFDM system under frequency-selective channels, a massive MIMO-OFDM system, in which the BS has a large number of antennas, may suffer from high computational complexity for PAPR reduction by the PCCNC. We emphasize the following reasons why the conventional PCCNC requires a high computational complexity in massive MIMO-OFDM systems. The number of real multiplications is used to evaluate the computational complexity in this study.

- Step 1 comprises the calculations of the null space $\mathbf{V}_k$ and projection matrix $\mathbf{V}_k\mathbf{V}_k^H$ for all $k = 1, \ldots, K$. The number of real multiplications in these calculations is proportional to the cube of the number of transmitter antennas. Thus, in a massive MIMO scenario, step 1 results in a very high computational complexity.
- Step 2 requires the projection of $\widetilde{\mathbf{w}}_k^{(q)}$ onto the null space in the MIMO channel for all $k = 1, \ldots, K$ in (11). Equation (11) requires $4KN^2$ real multiplications per iteration, which increases quadratically with the number of transmitter antennas N. Moreover, in the PCCNC, for a significant PAPR reduction, step 2 requires many iterations, *e.g.*, $Q = 1000$ iterations. Consequently, high computational complexity is required for sufficient PAPR reduction because step 2 involves $O(4KN^2Q)$ real multiplications.
- The addition of the average PC signal vector suppresses the peak power only once per iteration using the abundant degrees of freedom (DoFs) of a massive MIMO. Therefore, there is room for improvement when exploiting the abundant DoFs of a massive MIMO.

To address these problems, we propose two parallel techniques for reducing computational complexity while enhancing the PAPR reduction capability of the PCCNC.

IV. PROPOSED TWO PARALLEL TECHNIQUES

A. PARALLEL PCCNC WITH THE LOW-DIMENSIONAL NULL SPACE

To address these problems, we propose a parallel PCCNC with a low-dimensional null space. In particular, to reduce the computational complexity, the transmitter antennas jointly considered in the PCCNC are divided into antenna blocks. Moreover, the peak powers at different times are simultaneously suppressed per iteration owing to the independent parallel PCCNC for each antenna block.

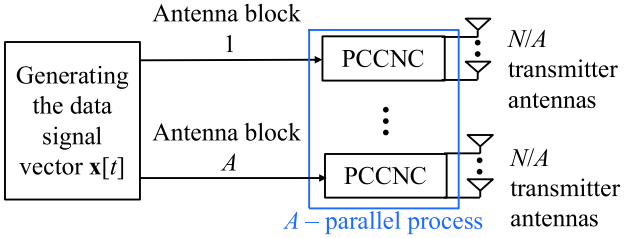

FIGURE 4. Block diagram of the parallel PCCNC with the low-dimensional null space.

Fig. 4 presents a block diagram of a parallel PCCNC with a low-dimensional null space. Let A denote the number of antenna blocks. The number of transmitter antennas per antenna block is N/A, where A satisfies $N/A > M$ and causes N/A to be an integer.

The antenna block a consists of the $(a–1)(N/A)+1$-th to the $a(N/A)$-th transmitter antennas. Thus, at the q-th iteration, the PCCNC in antenna block a is applied to the (N/A)-dimension vector consisting of the elements from the $(a-1)(N/A)+1$-th element to the $a(N/A)$-th element in $\mathbf{x}^{(q)}[t]$, which is represented as

$$\begin{aligned}\mathbf{x}_a^{(q)}[t] &= \left[x_{a,1}^{(q)}[t] \quad \cdots \quad x_{a,N/A}^{(q)}[t]\right]^T \\ &= \left[x_{(a-1)N/A+1}^{(q)}[t] \quad \cdots \quad x_{aN/A}^{(q)}[t]\right]^T. \end{aligned} \tag{14}$$

The $M \times (N/A)$-dimensional MIMO channel matrix of antenna block a associated with the k-th subcarrier is denoted as $\mathbf{H}_{k,a}$. As $N/A > M$, the $(N/A) \times (N/A–M)$-dimensional null space in the MIMO channel of antenna block a associated with k-th subcarrier exists as $\mathbf{V}_{k,a}$, such that $\mathbf{H}_{k,a}\mathbf{V}_{k,a} = \mathbf{O}$. All the $(N/A–M)$ column vectors in $\mathbf{V}_{k,a}$ are orthonormalized with each other.

In antenna block a at the q-th iteration, the target time index $\tau_a^{(q)}$ is determined depending on $\mathbf{x}_a^{(q)}[t]$, where $x_{a,n}^{(q)}[t]$ for all $n = 1, \ldots, N/A$ and $t = 0, \ldots, F-1$ has the maximum power over the power threshold P_{th}. By adding the PC signal vectors to all A antenna blocks, the PAPR is reduced as follows:

$$\overline{\mathbf{p}}_a^{(q)}[t] = \frac{1}{K}\sum_{k=1}^{K} \mathbf{w}_{k,a}^{(q)} g\left[t - \tau_a^{(q)}\right], \tag{15}$$

$$\mathbf{x}^{(q+1)}[t] = \begin{bmatrix}\mathbf{x}_1^{(q)}[t] \\ \vdots \\ \mathbf{x}_A^{(q)}[t]\end{bmatrix} + \begin{bmatrix}\overline{\mathbf{p}}_1^{(q)}[t] \\ \vdots \\ \overline{\mathbf{p}}_A^{(q)}[t]\end{bmatrix}, \tag{16}$$

where $\overline{\mathbf{p}}_a^{(q)}[t]$ is the (N/A)-dimensional average PC signal vector of antenna block a. $\mathbf{w}_{k,a}^{(q)}[t]$ is the (N/A)-dimensional BF vector of the PC signal vector of antenna block a associated with the k-th subcarrier, which is given by $\mathbf{w}_{k,a}^{(q)} = \mathbf{V}_{k,a}\mathbf{V}_{k,a}^H\widetilde{\mathbf{w}}_{k,a}^{(q)}$. $\widetilde{\mathbf{w}}_{k,a}^{(q)} = [\widetilde{w}_{k,a,1}^{(q)} \quad \cdots \quad \widetilde{w}_{k,a,N/A}^{(q)}]^T$ is the ideal BF vector of the PC signal of antenna block a associated with the k-th subcarrier in terms of the PAPR reduction as in (9). Each element of $\widetilde{w}_{k,a,n}^{(q)}$ is obtained in the same manner as that in the case of (10), using the phase of $x_{a,n}^{(q)}[\tau_a^{(q)}]$.

As the number of transmitter antennas jointly considered in the PCCNC is decreased by $1/A$ in a massive MIMO, the required number of real multiplications is significantly reduced for steps 1 and 2. In addition, the number of iterations required for realizing a sufficient PAPR reduction can be reduced owing to the simultaneous parallel suppression of the peak powers at different times in each antenna block.

B. PARALLEL PCCNC WITH SUPPRESSION OF MULTIPLE PEAKS

As another approach to reducing the required computational complexity in the PAPR reduction process, we propose a parallel PCCNC that simultaneously suppresses multiple peaks in each iteration. This method can be incorporated into the method described in Section IV-A. For convenience, we hereafter explain this for the case wherein $A = 1$, thus denoting $\mathbf{V}_{k,a}$ as $\mathbf{V}_k$. In particular, the average PC signal vector is obtained via an averaging process for the K/L PC signal vectors $\mathbf{p}_k^{(q)}[t]$, and L average PC signal vectors are added to suppress the peaks at L times per iteration. The aim of this approach is to reduce the required number of iterations of the PCCNC.

At the q-th iteration, the L target time indices $\tau_1^{(q)}, \ldots, \tau_L^{(q)}$ used to suppress the peak powers are determined based on $\mathbf{x}^{(q)}[t]$. Moreover, $\tau_1^{(q)}, \ldots, \tau_L^{(q)}$ are the time indices, where $x_n^{(q)}[t]$ for all $n = 1, \ldots, N$ and $t = 0, \ldots, F-1$ exhibits L maximum powers in the increasing order, which is over the power threshold P_{th} for the PCCNC. It should be noted that the proposed approach does not impose a constraint on the minimum time difference between the L selected target time indexes for PAPR reduction at each iteration, unlike the approach in [21]. The PC signal vector associated with the k-th subcarrier $\mathbf{p}_k^{(q)}[t]$ is denoted as

$$\mathbf{p}_k^{(q)}[t] = \mathbf{w}_k^{(q)} g_k\left[t - \tau_l^{(q)}\right], \tag{17}$$

where $l = 1, \ldots, L$ and $k = 1 + (l-1)K/L, \ldots, lK/L$. $\mathbf{w}_k^{(q)}$ denotes the BF vector associated with the k-th subcarrier, where $k = 1 + (l-1)K/L, \ldots, lK/L$ and can be obtained based on (10) and (11).

The average PC signal $\overline{\mathbf{p}}_l^{(q)}[t]$ for suppressing the peak power at time $\tau_l^{(q)}$ is denoted as

$$\overline{\mathbf{p}}_l^{(q)}[t] = \frac{1}{K/L}\sum_{k=1+(l-1)K/L}^{lK/L} \mathbf{p}_k^{(q)}[t]. \tag{18}$$

By adding $\overline{\mathbf{p}}_1^{(q)}[t], \ldots, \overline{\mathbf{p}}_L^{(q)}[t]$, the L peaks at times $\tau_1^{(q)}, \ldots, \tau_L^{(q)}$ can be suppressed simultaneously as follows:

$$\mathbf{x}^{(q+1)}[t] = \mathbf{x}^{(q)}[t] + \sum_{l=1}^{L} \overline{\mathbf{p}}_l^{(q)}[t]. \tag{19}$$

Therefore, in the proposed parallel PCCNC with the suppression of multiple peaks, the number of iterations for sufficient PAPR reduction is reduced, while the required number of real multiplications for each iteration is the same as that for the conventional PCCNC.

TABLE 2. Simulation parameters.

Number of transmitter antennas, N	Parameterized from 100 to 1000
Number of receiver antennas, M	4
Number of subcarriers, K	64
Number of FFT/IFFT points, F	256
Subcarrier modulation	64-QAM
BF of the data signal	Zero-forcing
Channel model	Six-path Rayleigh fading No fading correlations between any pair of transmitter and receiver antennas
Delay spread	80.4-μs rms
Channel estimation	Ideal

V. SIMULATION RESULTS

A. SIMULATION PARAMETERS

We evaluate the PAPR reduction capability and computational complexity using computer simulations. Table 2 lists the major simulation parameters used in this study.

Unless otherwise specified, we assume an uncoded MU massive MIMO-OFDM system, wherein a BS with $N = 100$ transmitter antennas simultaneously serves $M = 4$ single-antenna users. Furthermore, the ZF-based BF is applied to the data stream to completely eliminate the MUI. We consider an OFDM signal with $K = 64$ subcarriers and a subcarrier spacing of 60 kHz. The number of FFT/IFFT points F is set as 256, which corresponds to a four-times oversampling in the time domain for the accurate measurement of the PAPR levels [26]. For the data modulation scheme, we use 64-ary QAM (64-QAM) with Gray mapping. The channel model is assumed to comprise a six-pass Rayleigh fading with an 80.4-μs root mean square (rms) delay spread, where the antennas have no correlation. The channel estimation is assumed to be ideal. The transmission signals are amplified using an ideal linear power amplifier. The number of channel trials is fixed at 1000 in our simulations. To compare all the methods fairly, the transmission signal power after the PAPR reduction is normalized to one. At the q-th iteration, the power threshold P_{th} is defined as the signal power threshold normalized by the total power of the transmission signal $\mathbf{x}^{(q)}[t]$ over all the transmitter antennas and one OFDM symbol duration. In this study, P_{th} is set as 4 dB for all the iterations.

The PAPR of the transmission signal at the q-th iteration $\mathbf{x}^{(q)}$ is defined as the ratio of the highest peak power to its average power over all the transmitter antennas and one OFDM symbol duration, which is denoted as

$$PAPR = \frac{\max\limits_{0\le t\le F-1, 1\le n\le N}\left[\left|x_n^{(q)}[t]\right|^2\right]}{\sum_{t=0}^{F-1}\left\|\mathbf{x}^{(q)}[t]\right\|_2^2/NF}. \tag{20}$$

In addition, we evaluate the cubic metric (CM) [27], which is defined as

$$CM = \frac{20\log(v_{\text{rms}}) - 1.52}{1.85}, \tag{21}$$

TABLE 3. The number of real multiplications for the proposed PCCNC.

PAPR reduction method	Process		Number of real multiplications
PCCNC	Step 1	Calculating the null space $\mathbf{V}_{k,a}$	$K(4A\,(N/A)^3+2A\,(N/A)^2)$
		Calculating the projection matrix $\mathbf{V}_{k,a}\mathbf{V}_{k,a}^H$	$K(4A\,(N/A)^2(N/A-M))$
	Step 2	Generating the BF vecor $\mathbf{w}_k$ of the PC signal	$QK(4A\,(N/A)^2+4N)$
		Generating the PC signal vector	$QKNF$

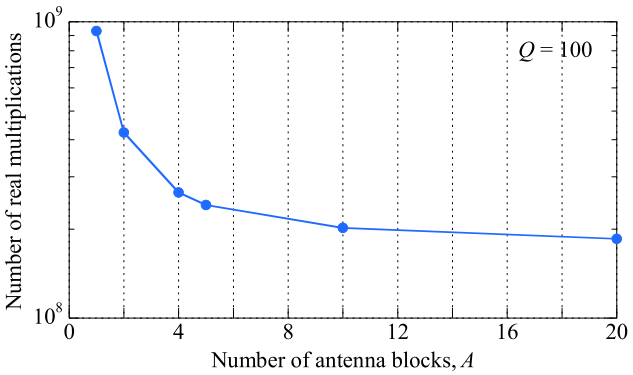

FIGURE 5. The number of real multiplications for proposed PCCNC described in Section IV-A as a function of the number of antenna blocks.

where v_{rms} is the root mean squared value of the instantaneous cubic amplitude for each symbol, normalized by the average amplitude of the input signal. In (21), 1.52 and 1.85 are empirical factors.

B. EVALUATION OF PARALLEL PCCNC WITH LOW-DIMENSIONAL NULL SPACE

In Section IV-A, we demonstrate the performance of the proposed parallel PCCNC with a low-dimensional null space. Table 3 lists the number of real multiplications with Q iterations of the PCCNC, which can be denoted as a function of N, M, K, Q, F, and A. It should be noted that the proposed parallel PCCNC with a low-dimensional null space for $A = 1$ is equivalent to the conventional PCCNC in Section III.

Fig. 5 presents the number of real multiplications for the proposed PCCNC described in Section IV-A as a function of A, where $Q = 100$. Fig. 5 shows that the number of real multiplications for the proposed PCCNC decreases as A increases. In particular, the proposed method with $A = 5$ reduces the number of real multiplications by approximately 38% compared to the conventional PCCNC. This is because the numbers of real multiplications for the processes in steps 1 and 2 increase proportionally to the cube and square of the number of transmitter antennas jointly considered in the PCCNC and N/A, respectively.

Fig. 5 shows that the proposed parallel PCCNC with a low-dimensional null space reduces the number of real multiplications as A increases. The dimensions of the null space also decrease as A increases. The decrease in the

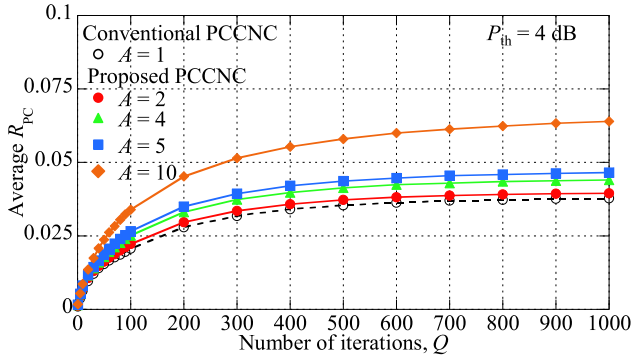

FIGURE 6. The average R_{PC} as a function of the number of iterations for the proposed parallel PCCNC with low-dimensional null space.

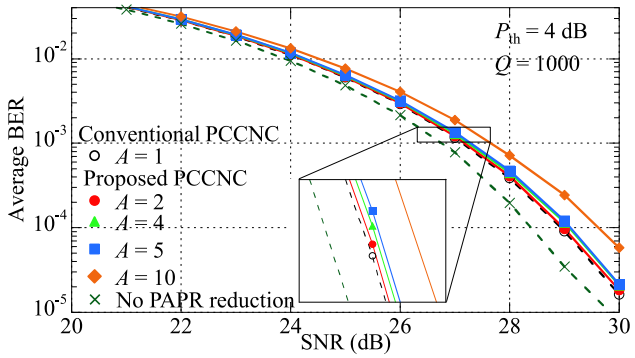

FIGURE 7. The average BER performance of the proposed parallel PCCNC with low-dimensional null space.

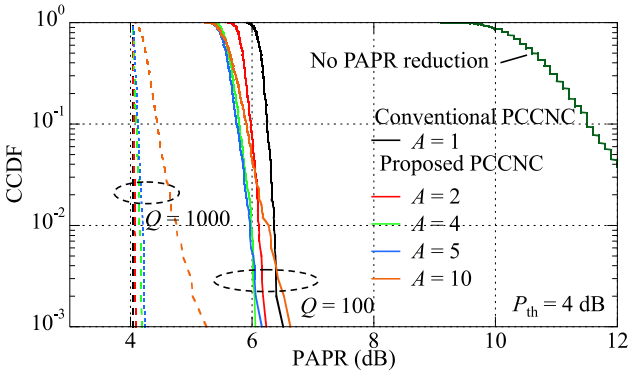

FIGURE 8. The CCDF of the PAPR for the proposed parallel PCCNC with a low-dimensional null space.

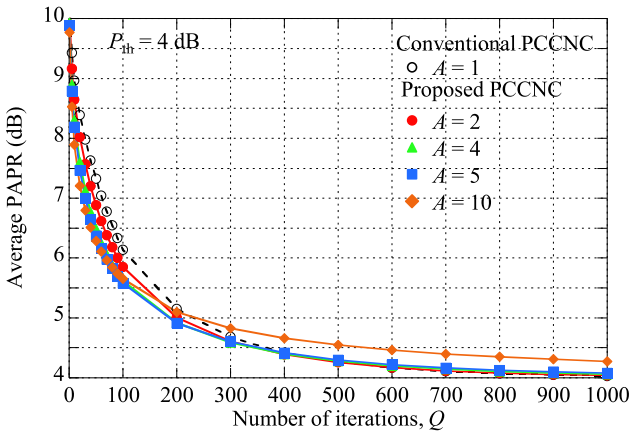

FIGURE 9. The average PAPR as a function of the number of iterations for the proposed parallel PCCNC with a low-dimensional null space.

dimensions of the null space may degrade the PAPR reduction capability. In the following section, we evaluate the relationship between A and the PAPR reduction capability.

To clarify the influence of a decrease in the dimension of the null space on the transmission quality, we define the ratio of the total PC signal power up to the q-th iteration to the transmission signal power R_{PC}, which is given by

$$R_{\mathrm{PC}} = \frac{\sum_{t=0}^{F-1} \left\| \sum_{q=1}^{Q} \overline{\mathbf{p}}^{(q)}[t] \right\|_2^2}{\sum_{t=0}^{F-1} \left\| \mathbf{x}^{(q)}[t] \right\|_2^2}. \tag{22}$$

Figs. 6 and 7 present the average R_{PC} as a function of Q and the average BER as a function of the signal-to-noise ratio (SNR) when $Q = 1000$, respectively. The SNR at the q-th iteration is defined as

$$SNR = \frac{\sum_{t=0}^{F-1} \left\| \mathbf{x}^{(q)}[t] \right\|_2^2}{N_0}. \tag{23}$$

In Figs. 6 and 7, the dotted black line indicates the conventional PCCNC with $A = 1$, and the red, green, blue, and orange lines indicate the proposed PCCNC with $A = 2$, 4, 5, and 10, respectively. In Fig. 7, the BER performance without a PAPR reduction is represented as an ideal case. As shown in Fig. 7, by setting a large A, the average R_{PC} of the proposed PCCNC becomes larger than that of the conventional PCCNC, *i.e.*, the power of the PC signals increases. This is because, as A increases, the proportion of streams corresponding to the null space among all the streams decreases, and the power loss required to cancel the interference with the data stream by restricting the PC signals within the null space increases. As shown in Fig. 7, the BER performance of the proposed PCCNC is degraded as A increases. This is because, as the transmission power consumption for the PC signal transmission increases, as shown in Fig. 6, the transmission power consumption for the data signal transmission is reduced. However, the BER performances for $A = 2$, 4, and 5 are slightly degraded compared with those of the conventional PCCNC, which uses a very high-dimensional null space. It can be confirmed that the proposed parallel PCCNC with $A = 2$, 4, and 5 has sufficient null space dimensions in terms of PAPR reduction.

To analyze the performance of the PAPR reduction, Figs. 8 and 9 present the complementary cumulative distribution function (CCDF) of the PAPR when $Q = 100$ and 1000, and the average PAPR as a function of the number of iterations of PCCNC Q, respectively. As shown in Fig. 8, when many iterations are acceptable, the PAPR is sufficiently reduced for P_{th} except when $A = 10$. However, when the number of iterations is small, the proposed parallel PCCNC achieves a

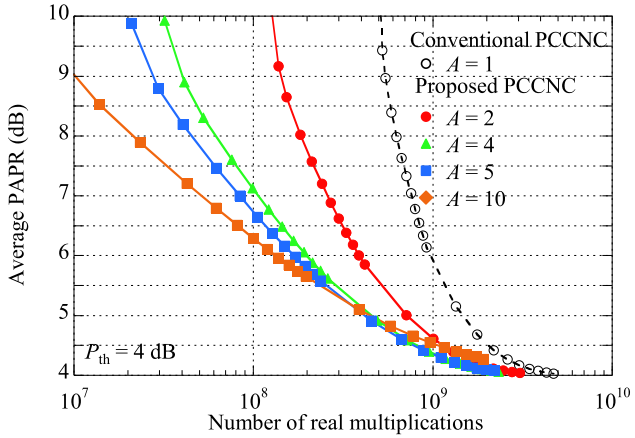

FIGURE 10. The average PAPR as a function of the number of real multiplications for the proposed parallel PCCNC with a low-dimensional null space.

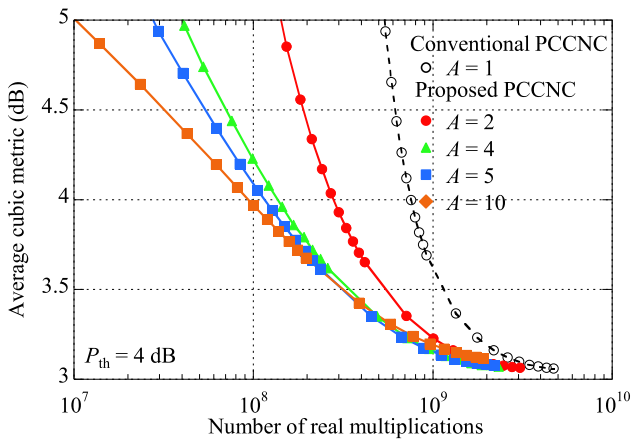

FIGURE 11. The average cubic metric as a function of the number of real multiplications for the proposed parallel PCCNC with a low-dimensional null space.

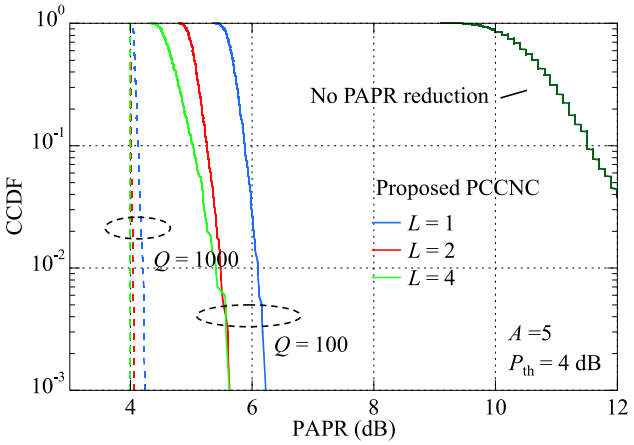

FIGURE 12. The CCDF of the PAPR for the proposed parallel PCCNC with suppression of multiple peaks.

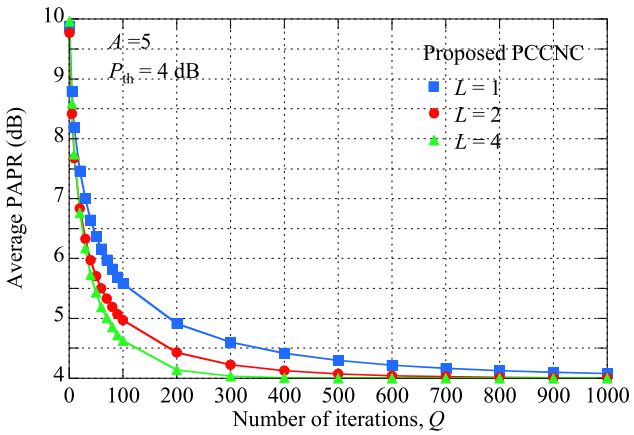

FIGURE 13. The average PAPR as a function of the number of iterations for the proposed parallel PCCNC with suppression of multiple peaks.

lower PAPR than the conventional PCCNC. This is because the peak powers that should be preferentially suppressed are suppressed with fewer iterations owing to the parallel PAPR reduction process for each antenna block. As shown in Fig. 9, the proposed parallel PCCNC converges the PAPR to approximately $P_{\text{th}} = 4$ dB with fewer iterations than the conventional PCCNC. This confirms the validity of the conclusion presented in Fig. 8. Thus, the proposed parallel PCCNC with a low-dimensional null space can achieve an efficient PAPR reduction.

For a comparison in terms of computational complexity, Figs. 10 and 11 present the average PAPR and cubic metric, respectively, as functions of the number of real multiplications for the PCCNC. As shown in Fig. 10, the proposed parallel PCCNC with a low-dimensional null space significantly reduces the number of real multiplications for meeting the required average PAPR. The proposed PCCNC with $A = 5$ is reduced by 63% compared with the conventional PCCNC at the required average PAPR of 4.5 dB. However, the PAPR of the proposed parallel PCCNC with $A = 10$ is likely to be higher than those of the other cases because the dimensions of the null space are insufficient for PAPR reduction. According to Fig. 11, these trends are also observed in the results of the average cubic metric. Therefore, we focused solely on evaluating the average PAPR. Furthermore, based on the above evaluations, we determined that the optimal number of antenna blocks is five, while considering the trade-off between the PAPR reduction capability and computational complexity.

C. EVALUATION OF PARALLEL PCCNC WITH SUPPRESSION OF MULTIPLE PEAKS

We evaluate the proposed parallel PCCNC with the suppression of multiple peaks in Section IV-B. To evaluate the convergence speed of the PAPR, Figs. 12 and 13 present the CCDF of the PAPR and average PAPR as a function of Q, respectively. The number of antenna blocks is set as five. The number of peaks to be suppressed at each antenna block per iteration is parameterized from 1 to 4. From Fig. 12, when many iterations are acceptable, the PAPR converges for P_{th} irrespective of L. In contrast, when the number of iterations is small, the proposed parallel PCCNC realizes

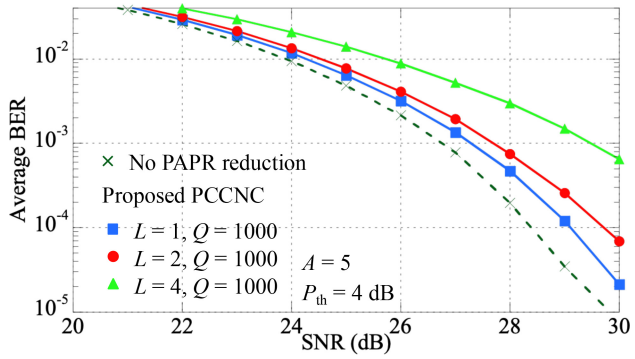

FIGURE 14. The average BER performance of the proposed parallel PCCNC with suppression of multiple peaks.

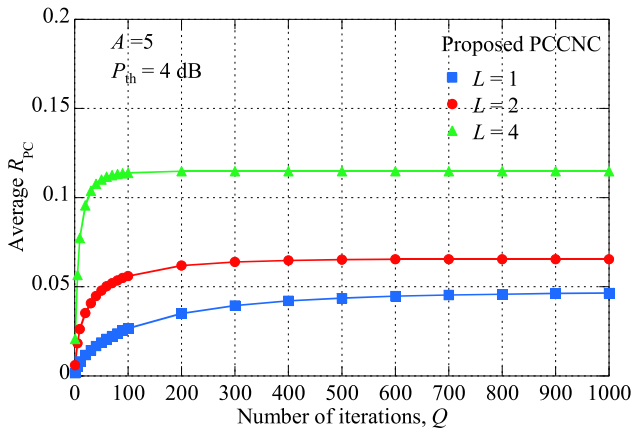

FIGURE 15. The average R_{PC} as a function of the number of iterations for the proposed parallel PCCNC with suppression of multiple peaks.

a lower PAPR as L increases. In addition, as shown in Fig. 13, the convergence speed of the PAPR increases when L increases. In particular, the proposed parallel PCCNC with $L = 2$ and 4 reduce the number of iterations by 47% and 64% at the required average PAPR of 4.5 dB, respectively. This result suggests that the proposed parallel PCCNC with the suppression of multiple peaks achieves efficient PAPR reduction as L increases.

An increase in L may cause the effective bandwidth of the PC signal to become narrower, thus resulting in the widening of the side lobe in the time domain. Hence, the power of the PC signal may increase owing to the wide side lobe. To measure the influence of the wide-side lobe of the PC signal on the transmission quality, Figs. 14 and 15 present the average BER as a function of the SNR, and the average R_{PC} as a function of the number of iterations, respectively. In Figs. 14 and 15, the blue, red, and green lines indicate the performances of the proposed PCCNC for $(L, Q) = (1, 1000)$, $(L, Q) = (2, 1000)$, and $(L, Q) = (4, 1000)$, respectively. As shown in Fig. 14, the average BER decreases as L increases. This is because, as L increases, the PC signal power increases owing to the wider side lobe of the PC signal. Moreover, Fig. 15 indicates that the average R_{PC} increases as L increases.

TABLE 4. The total number of real multiplications for the proposed PCCNC and MU-PP-GDm.

PAPR reduction method	Number of real multiplications
Proposed PCCNC	$K\{8A(N/A)^3+2A(1+2M+2Q)\ (N/A)^2+4NQ+QNF\}$
MU-PP-GDm[8]	$K(4N^3+2N^2)+16N^2M+32NM^2+36M^3+Q(8NF\log(F)+8KN^2)$

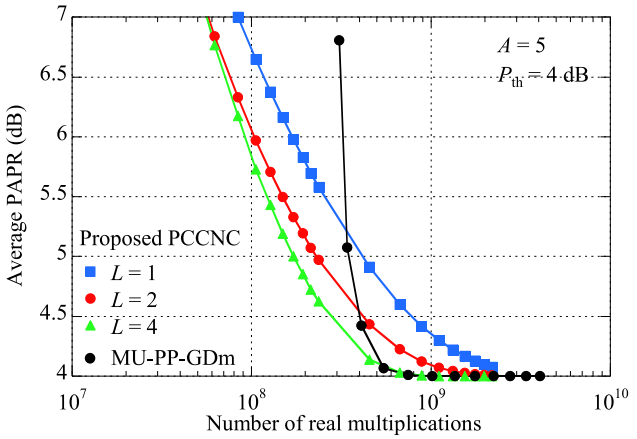

FIGURE 16. The average PAPR as a function of the number of real multiplications for the proposed PCCNC and MU-PP-GDm.

D. COMPARISON WITH MU-PP-GDM ALGORITHM

Finally, we compare the performance of a PC signal-based PAPR reduction method using the null space in the MIMO channel with that of an existing method, namely, MU-PP-GDm [8]. MU-PP-GDm transmits the PC signal only to the null space in the MIMO channel, in a manner similar to the PCCNC. However, this method is based on the gradient descent approach and can realize a significant PAPR reduction. However, this necessitates high computational complexity owing to the use of the SVD for the channel matrix of all the subcarriers. Moreover, in [8], because MU-PP-GDm uses a high-dimensional null space, which is similar to the conventional PCCNC, a high computational complexity is required for the calculation of the null space in the MIMO channel. In the following, we demonstrate that the proposed PCCNC has a significant PAPR reduction capability with low computational complexity compared to MU-PP-GDm.

Table 4 lists the total number of real multiplications for our proposed method and MU-PP-GDm [8]. The MU-PP-GDm requires FFT/IFFT operations for each iteration and SVD once, which results in $8NF\log(F) + 8KN^2$ real multiplications for each iteration and $16N^2M + 32NM^2 + 36\ M^3$ real multiplications, respectively. As shown in Table 4, the computational complexity of the MU-PP-GDm is directly proportional to the cube of the number of transmitter antennas. This indicates that the proposed PCCNC has the potential to outperform the MU-PP-GDm in terms of computational complexity.

Figs. 16 and 17 present the average PAPR as a function of the number of the real multiplications and BER performance.

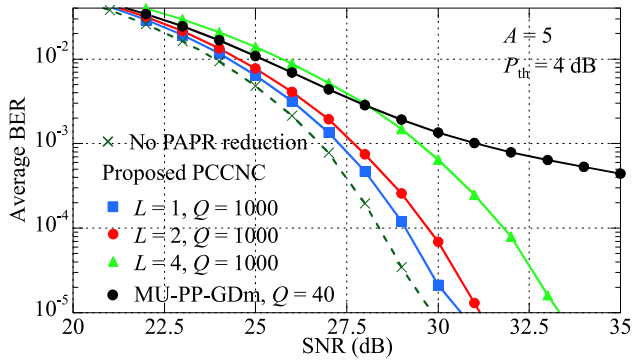

FIGURE 17. The average BER performance of the proposed PCCNC and MU-PP-GDm.

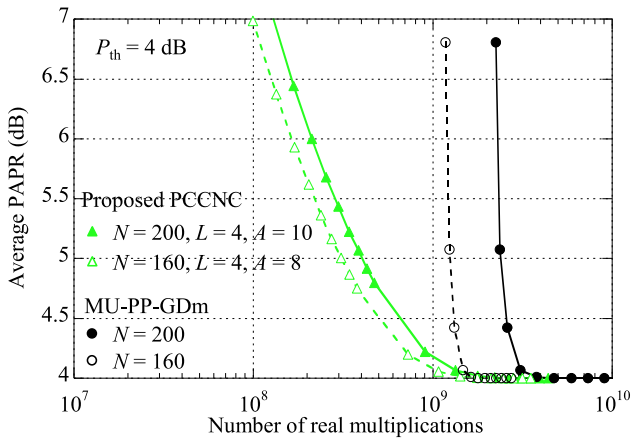

FIGURE 18. The average PAPR as a function of the number of real multiplications for the proposed PCCNC and MU-PP-GDm when $N = 160$ and $N = 200$.

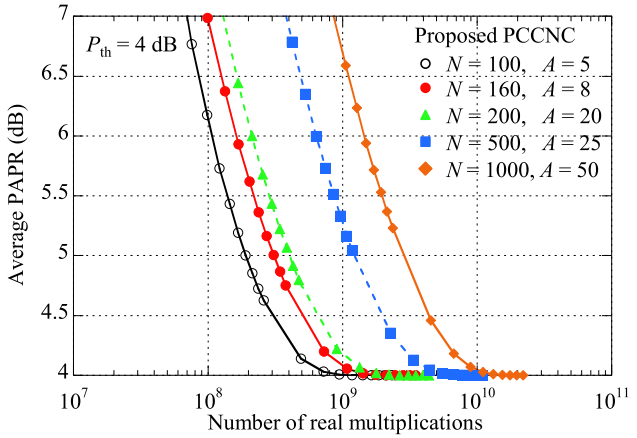

FIGURE 19. The average PAPR as a function of the number of real multiplications for the proposed PCCNC when N varies from 100 to 1000.

The blue, red, and green lines indicate the performances for $L = 1$, 2, and 4, respectively. Fig. 17 presents the BER performance after the convergence of the PAPR reduction. The black line indicates the performance of MU-PP-GDm. As shown in Fig. 16, the proposed parallel PCCNC reduces the number of real multiplications compared with the MU-PP-GDm. In particular, at the required average PAPR of 4.5 dB, the proposed parallel PCCNC for $L = 4$ reduces the number of real multiplications by approximately 21% compared to the MU-PP-GDm, which requires the same number of real multiplications as the proposed parallel PCCNC with $L = 2$. As shown in Fig. 17, the proposed PCCNC with $L = 1$ and 2 can suppress the BER performance loss irrespective of the SNR. Moreover, while the performance gap between the proposed PCCNC with $L = 4$ and MU-PP-GDm is small, the average BER performance of the proposed PCCNC improves when the SNR is greater than 28 dB. Therefore, the proposed PCCNC has a superior PAPR reduction capability with lower computational complexity as compared to the MU-PP-GDm.

We evaluate the impact of the number of transmitter antennas on the average PAPR of the proposed and conventional methods. Hereafter, we set the values of N/A and L as 20 and 4, respectively. Fig. 18 presents the average PAPR as a function of the number of real multiplications for the proposed PCCNC and MU-PP-GDm when $N = 160$ and $N = 200$. As shown in the figure, the proposed PCCNC can suppress the increase in the required real multiplications to achieve a low average PAPR, *e.g.*, 4.5dB, compared to MU-PP-GDm. Moreover, Fig. 19 presents the average PAPR as a function of the number of real multiplications for the proposed PCCNC when N varies from 100 to 1000. This result indicates that the performance of the proposed parallel PCCNC is comparable to that of MU-PP-GDm for $N = 200$ even when $N = 500$. Although the proposed method has a lower computational complexity than the state-of-the-art, a further complexity reduction for handling ultra-massive MIMO scenarios is left to future research.

VI. CONCLUSION

In this study, we investigated two parallel schemes for reducing the computational complexity of PAPR reduction using the null space in a MIMO channel, which is referred to as PCCNC. We first developed a scheme to exploit the low-dimensional null space by dividing the transmitter antennas jointly considered in the PCCNC. This reduces the computational complexity because the sizes of the matrices and vectors are reduced. Moreover, the scheme can be used to perform PCCNC simultaneously for each antenna block to enhance the efficiency of the PAPR reduction. To further reduce the computational complexity, we introduced a scheme to suppress multiple peaks at each iteration using PC signals that have multiple peaks in the time domain. The combination of these two schemes facilitated a tradeoff between the PAPR performance and computational complexity. The algorithmic design for ultra-massive MIMO scenarios and the investigation of the impact of antenna correlation are left to future research.

REFERENCES

[1] Z. Zhang et al., "6G wireless networks: Vision, requirements, architecture, and key technologies," *IEEE Veh. Technol. Mag.*, vol. 14, no. 3, pp. 28–41, Sep. 2019.

[2] T. L. Marzetta, "Noncooperative cellular wireless with unlimited numbers of base station antennas," *IEEE Trans. Wireless Commun.*, vol. 9, no. 11, pp. 3590–3600, Nov. 2010.
[3] H. Papadopoulos, C. Wang, O. Bursalioglu, X. Hou, and Y. Kishiyama, "Massive MIMO technologies and challenges towards 5G," *IEICE Trans. Commun.*, vol. E99-B, no. 3, pp. 602–621, Mar. 2016.
[4] C. Ni, Y. Ma, and T. Jiang, "A novel adaptive tone reservation scheme for PAPR reduction in large-scale multi-user MIMO-OFDM systems," *IEEE Wireless Commun. Lett.*, vol. 5, no. 5, pp. 480–483, Oct. 2016.
[5] H. Prabhu, O. Edfors, J. Rodrigues, L. Liu, and F. Rusek, "A low-complex peak-to-average power reduction scheme for OFDM based massive MIMO systems," in *Proc. 6th ISCCSP*, Athens, Greece, 2014, pp. 114–117.
[6] C. Studer and E. G. Larsson, "PAR-aware large-scale multi-user MIMO-OFDM downlink," *IEEE J. Sel. Areas Commun.* vol. 31, no. 2, pp. 303–313, Feb. 2013.
[7] H. Bao, J. Fang, Q. Wan, Z. Chen, and T. Jiang, "An ADMM approach for PAPR reduction for large-scale MIMO-OFDM systems," *IEEE Trans. Veh. Technol.*, vol. 67, no. 8, pp. 7407–7418, Aug. 2018.
[8] R. Zayani, H. Shaiek, and D. Roviras, "PAPR-aware massive MIMO-OFDM downlink," *IEEE Access*, vol. 7, pp. 25474–25484, 2019.
[9] S. Taner and C. Studer, "Alternating projections method for joint precoding and peak-to-average-power ratio reduction," in *Proc. IEEE WCNC*, Glasgow, Scotland, 2023, pp. 1–7.
[10] M. Kim, W. Lee, and D.-H. Cho, "A novel PAPR reduction scheme for OFDM system based on deep learning," *IEEE Commun. Lett.*, vol. 22, no. 3, pp. 510–513, Mar. 2018.
[11] R. Kuwahara and M. Ohta, "PAPR and OOBE suppression of OFDM signal using deep learning," in *Proc. IEEE 9th GCCE*, Kobe, Japan, 2020, pp. 905–906.
[12] A. Kalinov, R. Bychkov, A. Ivanov, A. Osinsky, and D. Yarotsky, "Machine learning-assisted PAPR reduction in massive MIMO," *IEEE Wireless Commun. Lett.*, vol. 10, no. 3, pp. 537–541, Mar. 2021.
[13] N. Chen and G. Zhou, "Superimposed training for OFDM: A peak-to-average power ratio analysis," *IEEE Trans. Signal Process.*, vol. 54, no. 6, pp. 2277–2287, Jun. 2006.
[14] K. C.-Hu, M. J. F.-G. García, and A. G. Armada, "Dual layers-superimposed training for joint channel estimation and PAPR reduction in OFDM," in *Proc. IEEE GLOBECOM*, Kuala Lumpur, Malaysia, 2023, pp. 4038–4043.
[15] R. Kimura, Y. Tajika, and K. Higuchi, "CF-based adaptive PAPR reduction method for block diagonalization-based multiuser MIMO-OFDM signals," in *Proc. IEEE 73rd VTC*, Budapest, Hungary, 2011, pp. 1–5.
[16] S. Inoue, T. Kawamura, and K. Higuchi, "Throughput/ACLR performance of CF-based adaptive PAPR reduction method for eigenmode MIMO-OFDM signals with AMC," *IEICE Trans. Commun.*, vol. E96-B, no. 9, pp. 2293–2300, Sep. 2013.
[17] Y. Matsumoto, K. Tateishi, and K. Higuchi, "Performance evaluations on adaptive PAPR reduction method using null space in MIMO channel for eigenmode massive MIMO-OFDM signals," in *Proc. 23rd APCC*, 2017, pp. 1–6.
[18] A. Ivanov, A. Volokhatyi, D. Lakontsev, and D. Yarotsky, "Unused beam reservation for PAPR reduction in massive MIMO system," in *Proc. IEEE 87th VTC*, Porto, Portugal, 2018, pp. 1–5.
[19] T. Suzuki, M. Suzuki, Y. Kishiyama, and K. Higuchi, "Complexity-reduced adaptive PAPR reduction method using null space in MIMO channel for MIMO-OFDM signals," *IEICE Trans. Commun.*, vol. E103-B, no. 9, pp. 1019–1029, Sep. 2020.
[20] L. Yamaguchi, N. Nonaka, and K. Higuchi, "PC-signal-based PAPR reduction using null space in MIMO channel for MIMO-OFDM signals in frequency-selective fading channel," in *Proc. IEEE 92nd VTC*, 2020, pp. 1–5.
[21] T. Suzuki, M. Suzuki, and K. Higuchi, "Parallel peak cancellation signal-based PAPR reduction method using null space in MIMO channel for MIMO-OFDM transmission," *IEICE Trans. Commun.*, vol. E104-B, no. 5, pp. 539–549, May 2021.
[22] J. Saito, N. Nonaka, and K. Higuchi, "PAPR reduction using null space in MIMO channel considering signal power difference among transmitter antennas," in *Proc. IEEE WCNC*, 2023, pp. 1–5.
[23] J. Saito, T. Hara, and K. Higuchi, "Peak cancellation signal-based parallel PAPR reduction method using low-dimensional null space in massive MIMO-OFDM," in *Proc. IEEE ICNC2024*, Big Island, HI, USA, 2024, pp. 539–549.
[24] T. Hino and O. Muta, "Adaptive peak power cancellation scheme under the requirements of ACLR and EVM for MIMO-OFDM systems," in *Proc. IEEE 23rd PIMRC*, Sydney, NSW, Australia, 2012, pp. 1974–1978.
[25] T. Kageyama, O. Muta, and H. Gacanin, "An adaptive peak cancellation method for linear-precoded MIMO-OFDM signals," in *Proc. IEEE 26th PIMRC*, 2015, pp. 271–275.
[26] M. Sharif, M. Gharavi-Alkhansari, and B. H. Khalaj, "On the peak-to-average power of OFDM signals based on oversampling," *IEEE Trans. Commun.*, vol. 51, no. 1, pp. 72–78, Jan. 2003.
[27] T. Kawamura, Y. Kishiyama, K. Higuchi, and M. Sawahashi, "Investigations on optimum roll-off factor for DFT-spread OFDM based SC-FDMA radio access in evolved UTRA uplink," in *Proc. IEEE ISWCS*, Valencia, Spain, 2006, pp. 383–387.

JUN SAITO (Graduate Student Member, IEEE) received the B.E. degree from the Tokyo University of Science, Noda, Japan, in 2022, where he is currently pursuing the M.E. degree with the Department of Electrical Engineering. His research interests include wireless communications.

TAKANORI HARA (Member, IEEE) received the B.E., M.E., and Ph.D. degrees in engineering from The University of Electro-Communications, Tokyo, Japan, in 2017, 2019, and 2022, respectively. Since April 2022, he has been with the Department of Electrical Engineering, Tokyo University of Science, Chiba, Japan, where he is currently an Assistant Professor. His current research interests are grant-free access, compressed sensing, and MIMO technologies.

KENICHI HIGUCHI (Senior Member, IEEE) received the B.E. degree from Waseda University, Tokyo, Japan, in 1994, and the Dr.Eng. degree from Tohoku University, Sendai, Japan, in 2002. In 1994, he joined NTT Mobile Communications Network, Inc. (currently, NTT DOCOMO, Inc.). While with NTT DOCOMO, Inc., he was engaged in the research and standardization of wireless access technologies for wideband DS-CDMA mobile radio, HSPA, LTE, and broadband wireless packet access technologies for systems beyond IMT-2000. In 2007, he joined the faculty of the Tokyo University of Science, where he is currently a Professor. His current research interests are in the areas of wireless technologies and mobile communication systems, including advanced multiple access, radio resource allocation, intercell interference coordination, multiple-antenna transmission techniques, signal processing, such as interference cancellation and turbo equalization, and issues related to heterogeneous networks using small cells. He was a co-recipient of the Best Paper Award of the International Symposium on Wireless Personal Multimedia Communications in 2004 and 2007, and the Best Paper Award from the IEICE in 2021, and a recipient of the Young Researcher's Award from the IEICE in 2003, the 5th YRP Award in 2007, the Prime Minister Invention Prize in 2010, and the Invention Prize of Commissioner of the Japan Patent Office in 2015. He is a Senior Member of IEICE.